A Mössbauer investigation of the dissociation of the $Nd_2Fe_{14}B$ phase

A Mössbauer investigation of the dissociation of the $Nd_2Fe_{14}B$ phase

J-M Le Breton and S Steyaert

Magnétisme et Applications, GMP UMR 6634 CNRS-Université de Rouen, Faculté des Sciences, 76821 Mont-Saint-Aignan Cedex, France

Abstract.   The dissociation process of the $Nd_2Fe_{14}B$ phase in a sintered $Nd_{16}Fe_{76}B_8$ powdered magnet was investigated between 300 and 650 °C. The oxidized powders were characterized by Mössbauer spectrometry and x-ray diffraction. The contributions of the dissociation products to the Mössbauer spectra were identified and the results interpreted consistently with previous transmission electron microscopy observations. The microstructure of the dissociated phase was characterized and found to depend on the oxidation temperature. For temperatures less than 400 °C, the microstructure consists in α-Fe nanograins (less than 10 nm in size, with a distorted structure) and Fe_3O_4 superparamagnetic particles (size less than 10 nm), mixed with amorphous or poorly crystallized Nd_2O_3 regions. For temperatures higher than 400 °C the microstructure consists in bigger α-Fe grains (their size being 100 nm or more), Fe_3O_4 precipitates (size less than 10 nm) and crystallized Nd_2O_3 precipitates. It appears that the presence of additives in sintered Nd–Fe–B magnets does not change the dissociation process. Apart from some contributions in very weak proportions in Co containing samples, the same contributions are detected, owing to the same reactions.

1. Introduction

During the last 12 years, the corrosion behaviour of Nd–Fe–B permanent magnets has been extensively studied either in warm humid air/steam [1–3] or at high temperature [4–6]. Sintered Nd–Fe–B magnets have a three phase microstructure ($Nd_2Fe_{14}B$, $Nd_{1.1}Fe_4B_4$ and an intergranular Nd-rich phase). The Nd-rich phase is the less corrosion resistant, being responsible for the poor corrosion resistance of Nd–Fe–B magnets under humid conditions [7]. The $Nd_2Fe_{14}B$ hard magnetic phase, responsible for the good intrinsic magnetic properties of the magnet, oxidizes at temperatures above 100 °C [8, 9]. The $Nd_{1.1}Fe_4B_4$ phase is good corrosion resistant, as its oxidation is not observed below 400 °C [5, 6].

   The oxidation mechanism of the $Nd_2Fe_{14}B$ hard magnetic phase was first characterized by transmission electron microscopy (TEM) on an $Nd_{16}Fe_{76}B_8$ magnet heated at 423 °C in ambient air [10]: the Nd is oxidized and the phase dissociates into α-Fe crystals, which grow epitaxially from the $Nd_2Fe_{14}B$ substrate. The orientation of the α-Fe crystals is intimately linked to the $Nd_2Fe_{14}B$ one. Electron diffraction analyses revealed that the oxidized $Nd_2Fe_{14}B$ grains are composed mainly of monocrystals of α-Fe having a common [111] crystallographic direction, most adjacent monocrystals being rotated 30° from each other. It was stated that the α-Fe monocrystals are typically several hundred nanometres in diameter, and contain fine precipitates, with a dispersion of size around 5 nm. According to electron diffraction analyses, these precipitates were considered to be hexagonal Nd_2O_3.

   Another TEM study made on a sintered Nd–Dy–Fe–Co–V–Al–B magnet heated at 110 °C under 100% relative humidity revealed that the microstructure of the dissociated $Nd_2Fe_{14}B$

phase is constituted of α-Fe nanocrystallites (mean size: 2 nm), organized in domains with the same crystallographic orientation [9]. The size of the domains is about 100 nm. It was stated that the α-Fe nanocrystallites are embedded in an amorphous neodymium oxide (Nd_2O_3).

As the microstructure of the dissociated $Nd_2Fe_{14}B$ phase is not clearly established, a complementary study is needed in order to characterize it accurately. Because Mössbauer spectrometry is a local probe of the iron atomic environment, the identification of the Mössbauer contributions to the spectrum of an oxidized magnet can help to characterize the microstructure of the dissociated phase.

In this study, the dissociation of the $Nd_2Fe_{14}B$ phase in sintered Nd–Fe–B magnets oxidized at high temperature (300–650 °C in ambient atmosphere) is investigated by ^{57}Fe Mössbauer spectrometry and x-ray diffraction. The microstructure is discussed as a function of both temperature and treatment time. An investigation of oxidized magnets containing additives (Co, Al, Nb, V, Mo) is also reported.

2. Experimental procedure

Several sintered Nd–Fe–B magnets with different compositions (table 1) were powdered by mechanical grinding and sieved (the diameter of the particles being less than 20 μm). The powders were heated in a conventional air furnace, in the 300–650 °C range for times up to 7 days. The oxidized powders were analysed by x-ray diffraction (XRD) and transmission ^{57}Fe Mössbauer spectrometry (TMS) at room temperature. Some Mössbauer spectra were recorded at 77 K.

Table 1. Nominal atomic compositions of the samples investigated.

Name	Composition
	$Nd_{16}Fe_{76}B_8$
DCVA	$Nd_{13.5}Dy_{1.5}Fe_{67}Co_5V_4B_8Al$
CVA	$Nd_{14}Fe_{69.6}Co_5V_3B_7Al_{1.4}$
CMA	$Nd_{14.4}Pr_{0.2}Fe_{69.7}Co_5Mo_{2.5}B_{7.2}Al$
DNA	$Nd_{13.9}Pr_{0.2}Dy_{0.4}Fe_{77.9}Nb_{0.7}B_{6.2}Al_{0.7}$

XRD analyses were performed by reflexion, in an evacuated chamber using a fast curved detector INEL CPS 120. The x-ray generator was equipped with a Co anticathode, using Co (Kα) radiation ($\lambda = 0.179\,09$ nm).

TMS analyses were performed using a conventional ^{57}Co source in a rhodium matrix. The samples contain about 10 mg cm^{-2} of natural iron. The isomer shift (relative to metallic α-Fe at room temperature), quadrupolar splitting, quadrupolar shift and hyperfine field are denoted δ, Δ, ε and B respectively. Estimated errors for the hyperfine parameters originate from the statistical errors σ given by the fitting program [11], taking 3σ.

3. Powders oxidized in the 300–650 °C temperature range

3.1. The dissociation products at 300 °C

In figure 1 are shown the Mössbauer spectra of a powdered $Nd_{16}Fe_{76}B_8$ magnet before oxidation and after oxidation at 300 °C for 12 hours. The Mössbauer spectrum of the unoxidized powder is fitted with the contributions of $Nd_2Fe_{14}B$ [12] and $Nd_{1.1}Fe_4B_4$ [13] phases. No more $Nd_2Fe_{14}B$ is detected in the spectrum of the oxidized powder, 12 hours being the time necessary for the complete dissociation of the $Nd_2Fe_{14}B$ phase at 300 °C [14]. The contributions used to fit this spectrum are displayed in figure 2, and the corresponding hyperfine parameters and
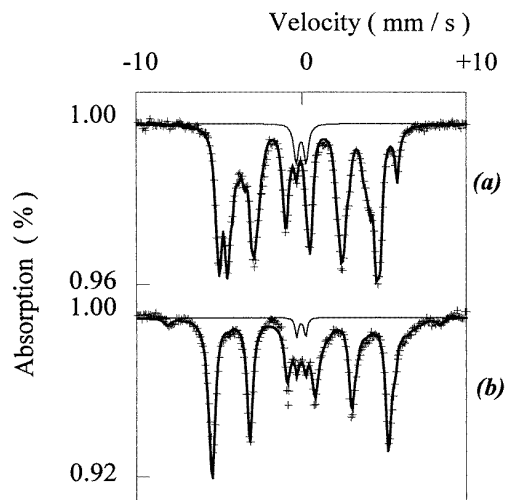
Figure 1. Room temperature Mössbauer spectra of the Nd$_{16}$Fe$_{76}$B$_8$ powder before (a) and after oxidation at 300 °C for 12 hours (b). The contribution of the Nd$_{1.1}$Fe$_4$B$_4$ phase is displayed.
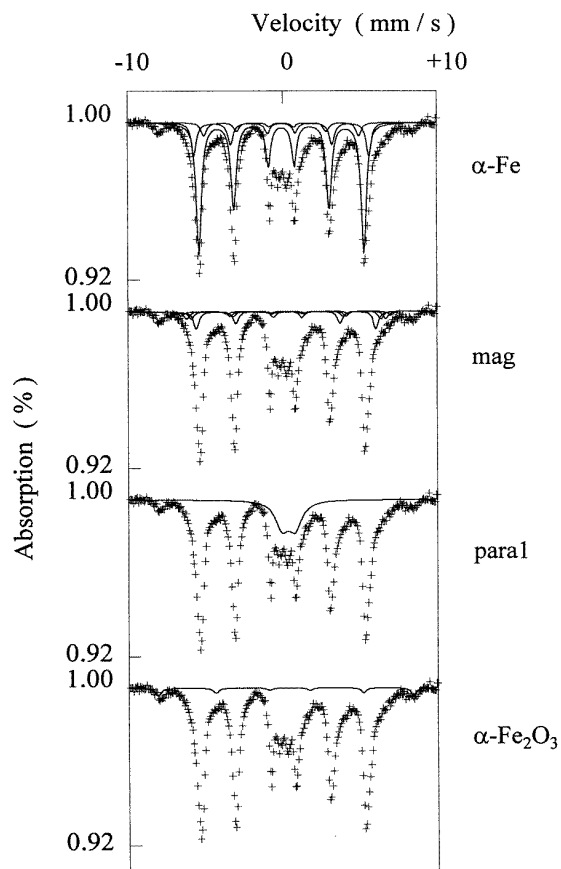

Figure 2. The contributions used to fit the room temperature Mössbauer spectrum of the Nd$_{16}$Fe$_{76}$B$_8$ powder oxidized at 300 °C for 12 hours.

Table 2. Hyperfine parameters and relative absorption areas ($\pm 1\%$) of the contributions to the Mössbauer spectra of the $Nd_{16}Fe_{76}B_8$ powder oxidized at 300 °C (for 12 hours) and in the 350–650 °C temperature range (for 2 hours). * means that the contribution was fitted using a distribution of hyperfine fields (B is the mean hyperfine field). † means that the contribution was fitted using a sextet ($B = 33.0 \pm 0.1$ T). The hyperfine parameters for Fe_3O_4 were fixed to the values obtained from the literature [15].

	Hyperfine parameters			Relative absorption area (%)							
Contribution	δ (mm s^{-1})	$2\varepsilon, \Delta$ (mm s^{-1})	B (T)	300 °C 12 h	350 °C 2 h	400 °C 2 h	450 °C 2 h	500 °C 2 h	550 °C 2 h	600 °C 2 h	650 °C 2 h
α-Fe	0.00 ± 0.02	0.00 ± 0.01	33.3	67*	58*	42*	26†	15†	3†	—	—
mag	0.34 ± 0.02	−0.10 ± 0.02	38.0	14*	14*	8*	—	—	—	—	—
α-Fe$_2$O$_3$	0.27 ± 0.04	−0.17 ± 0.05	51.4 ± 0.2	3	9	20	34	40	53	61	67
Fe$_3$O$_4$	0.26 0.67	−0.16 −0.20	49.0 46.0	—	—	5	9	12	10	0	—
Nd$_{1.1}$Fe$_4$B$_4$	0.03 ± 0.02	0.58 ± 0.04	—	3	4	4	5	4	1	0	—
Fe$_3$B	0.01 ± 0.04 −0.09 ± 0.04 0.11 ± 0.04	0.00 fixed 0.00 fixed 0.00 fixed	27.8 ± 0.2 26.2 ± 0.2 22.6 ± 0.2	—	—	—	—	—	5	5	5
NdFeO$_3$	0.36 ± 0.02	0.07 ± 0.02	43.2	—	—	—	—	7*	7*	14*	16*
para1	0.38 ± 0.05	0.73 ± 0.07	—	13	12	18	21	7	—	—	—
para2	1.33 ± 0.03	0.54 ± 0.07	—	—	3	3	5	2	—	—	—
para3	0.30 ± 0.02	1.05 ± 0.05	—	—	—	—	—	13	21	20	12

relative absorption areas are reported in table 2. It is worth mentioning that these contributions were used to fit the Mössbauer spectra of the same powder oxidized between 150 and 300 °C [14]. This indicates that the dissociation process of the $Nd_2Fe_{14}B$ phase is the same in this temperature range.

The α-Fe contribution is fitted with a discrete distribution of hyperfine fields, the mean hyperfine field value being 33.3 T. The width of the distribution is related to the poor crystallized nature of the α-Fe phase. The fact that the mean hyperfine field of α-Fe in the oxidized powders is slightly higher than that of pure α-Fe (33.0 T) can be related to the presence of strains, probably due to the presence of interstitial B atoms in the structure.

An unidentified magnetic contribution (namely mag) is fitted with a discrete distribution of hyperfine field, distinct from that of α-Fe, to account for the non-symmetric broadening at the basis of the α-Fe lines. Another fit with one large discrete distribution shows two maxima at 33 and 38 T (indicating two different kinds of environment around the Fe atoms) which correspond to the mean hyperfine fields of the two distinct distributions (figure 3). However, because such a fit does not account for the asymmetry of the broadening at the basis of the α-Fe lines, all the Mössbauer spectra presented here were fitted with two distinct distributions.

The α-Fe$_2$O$_3$ contribution is fitted, evidencing the oxidation of some α-Fe. The paramagnetic contribution of the $Nd_{1.1}Fe_4B_4$ phase is detected, showing that this phase is not oxidized
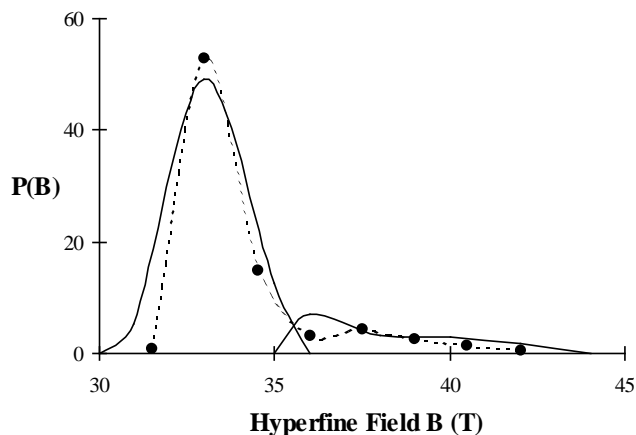
Figure 3. The two hyperfine field distributions (solid lines) used to fit the α-Fe and mag contributions. The single hyperfine field distribution (dotted line) is shown for comparison.

up to at least 300 °C, in agreement with previous work [5, 6]. One paramagnetic unidentified contribution (namely para1) is fitted to account for the broadening at the centre of the spectra.

Apart from the Nd$_{1.1}$Fe$_4$B$_4$ contribution, all the contributions correspond to the dissociation products of the Nd$_2$Fe$_{14}$B phase.

The XRD pattern of the oxidized Nd$_{16}$Fe$_{76}$B$_8$ powder is shown in figure 4. No more Nd$_2$Fe$_{14}$B peak is observed, a very broad α-Fe(110) peak being present instead. Some α-Fe$_2$O$_3$ peaks are observed as well. These observations are in agreement with the Mössbauer results. The main peak of the cubic Nd$_2$O$_3$ phase (c-Nd$_2$O$_3$) is detected, its presence being attributed to the oxidation of the Nd-rich phase [6].

3.2. Structural evolution of the dissociation products in the 350–650 °C range

With the aim of following the behaviour of the dissociation products during oxidation, and thus of obtaining more information on the structure of the dissociated phase, Nd$_{16}$Fe$_{76}$B$_8$ powders were oxidized for 2 hours in the 350–650 °C range.

The corresponding XRD patterns are shown in figure 4. As the temperature increases, several remarks can be made. First, the intensity of the broad α-Fe peak decreases as the intensities of the α-Fe$_2$O$_3$ peaks increase, in agreement with the oxidation of the α-Fe phase. At 500 °C, the α-Fe peak is sharp, indicating that a change in the structure of the α-Fe phase has occurred. At 550 °C, the intensity of the α-Fe peak is weak: the α-Fe phase is almost fully oxidized. Second, the Nd$_{1.1}$Fe$_4$B$_4$ peaks are no longer observed at 500 °C, indicating that this phase starts to oxidize at this temperature. Third, the main peaks of hexagonal Nd$_2$O$_3$ (h-Nd$_2$O$_3$) can be observed from about 500 °C. As this temperature corresponds to a change in the structure of the α-Fe phase, the appearance of the h-Nd$_2$O$_3$ peaks can be related to a change in the structure of the Nd$_2$O$_3$ amorphous regions (that is to the crystallization of amorphous Nd$_2$O$_3$), the Nd$_2$O$_3$ amorphous regions resulting from the dissociation of the Nd$_2$Fe$_{14}$B phase [9]. Fourth, from 500 °C, the peaks of NdFeO$_3$ are observed, indicating that some α-Fe$_2$O$_3$ phase reacts with c-Nd$_2$O$_3$ or h-Nd$_2$O$_3$ to form NdFeO$_3$.

The room temperature Mössbauer spectra of the oxidized Nd$_{16}$Fe$_{76}$B$_8$ powders are shown in figure 5. The hyperfine parameters and relative absorption areas of the different contributions used to fit the spectra are reported in table 2. Except for the Fe$_3$O$_4$ magnetic contribution, the
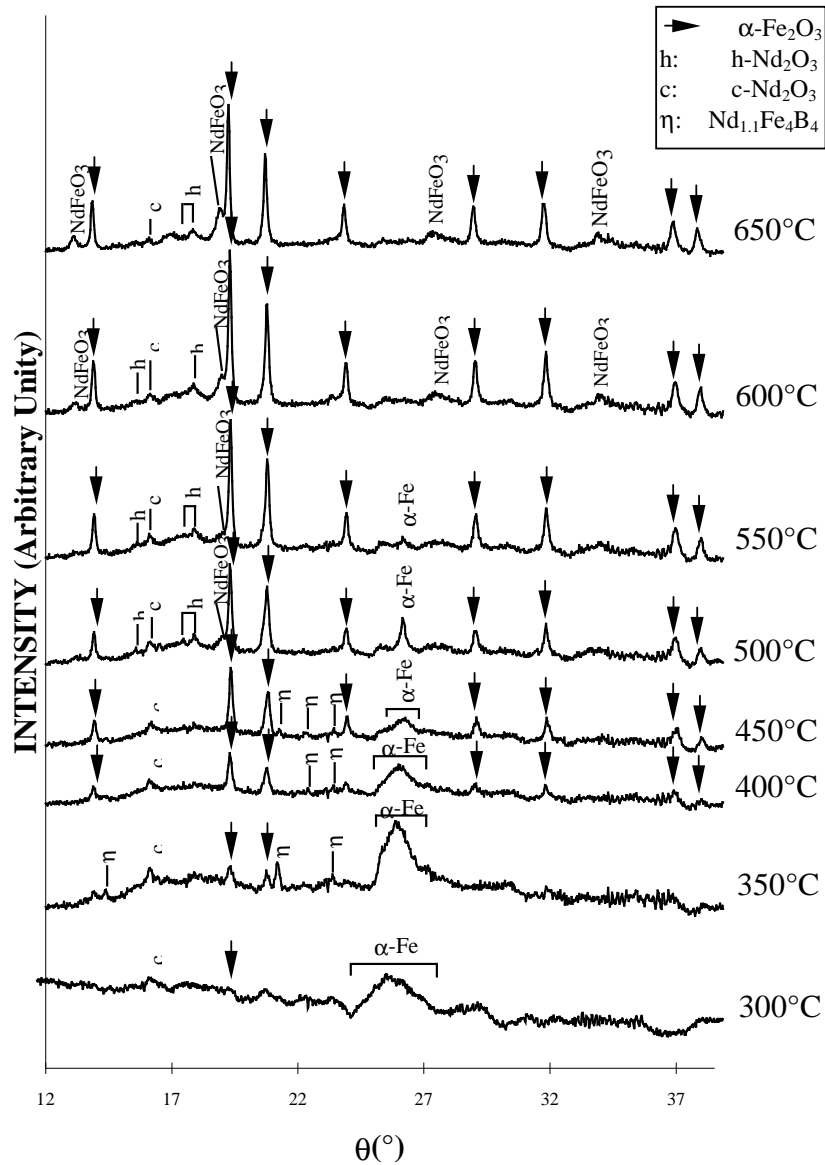
Figure 4. XRD patterns of the $Nd_{16}Fe_{76}B_8$ powder oxidized in the 300–650 °C range.

hyperfine parameters of the different phases were allowed to vary only in the spectra where their corresponding relative absorption area is maximum (errors for the hyperfine parameters are deduced from these fittings). The spectra were fitted by keeping constant the hyperfine parameters of the same phase in the different samples and allowing the relative areas to vary. The hyperfine parameters used for the Fe_3O_4 phase come from [15].

The Mössbauer spectrum of the powder oxidized at 350 °C was fitted with the same contributions as those used to fit the spectrum of the powder oxidized at 300 °C, and in addition a paramagnetic doublet (para2) with a weak relative area. With increasing temperature in the
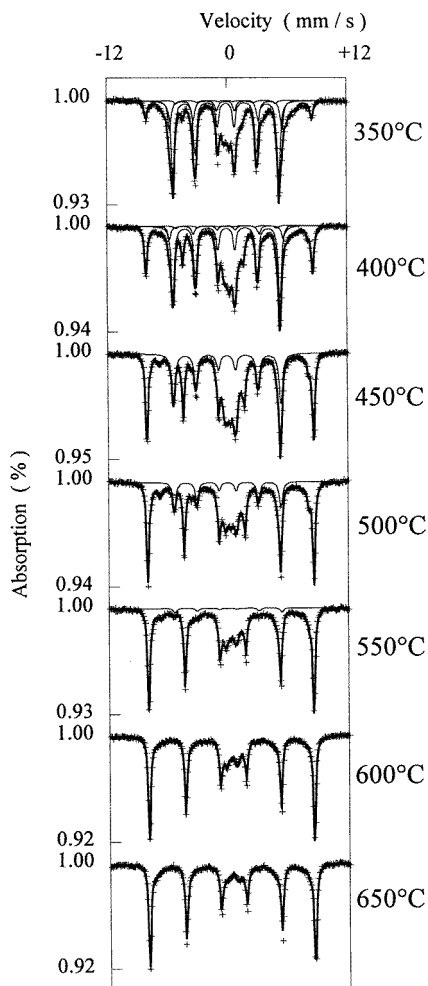
Figure 5. Room temperature Mössbauer spectra of the Nd$_{16}$Fe$_{76}$B$_8$ powder oxidized for 2 hours in the 350–650 °C temperature range. The contribution of the α-Fe phase is displayed.

350–500 °C range, the relative areas of both α-Fe and mag contributions decrease, as those of α-Fe$_2$O$_3$ and Fe$_3$O$_4$ increase, according to the oxidation of α-Fe. The relative area of the para1 doublet increases as well, indicating that this contribution could correspond to an iron oxide. The relative areas of the Nd$_{1.1}$Fe$_4$B$_4$ and para2 contributions remain constant, within the accuracy of the measurement. Between 500 and 550 °C, new contributions appear in the spectra, while some others disappear. The Fe$_3$O$_4$ relative area decreases from 500 °C and Fe$_3$O$_4$ disappears at 600 °C. The NdFeO$_3$ contribution appears and its relative area increases up to 650 °C. The Nd$_{1.1}$Fe$_4$B$_4$ contribution disappears at 550 °C, and this corresponds to the appearance of the Fe$_3$B contribution. This seems to indicate that Nd$_{1.1}$Fe$_4$B$_4$ oxidizes at 550 °C, resulting in the formation of Fe$_3$B, in agreement with the fact that the relative area of Fe$_3$B is equal to that of Nd$_{1.1}$Fe$_4$B$_4$. At 500 °C, the paramagnetic contributions para1 and para2 disappear and another paramagnetic contribution (namely para3) appears instead, suggesting that the para1 and para2 compounds transform into para3 due to an oxidation reaction.

4. Characterization of the Mössbauer contributions

As the hyperfine parameters of the unidentified contributions (mag, para1, para2 and para3) do not correspond to any Fe–B–O or Fe–B phase, further heat treatments were performed to allow their identification.

4.1. The magnetic contribution

As previous investigations showed that α-Fe nanograins are formed during the dissociation process of the $Nd_2Fe_{14}B$ phase [9], the mag contribution is attributed to Fe atoms located at the surface of the α-Fe nanograins while the α-Fe contribution corresponds to Fe atoms within the nanograins. The fact that both the isomer shift and the hyperfine field of the surface contribution are higher than those of the bulk contribution could be related to a reduced interfacial density at the surface of the nanograins, in agreement with theoretical calculations [16, 17], and to the fact that in the dissociated structure the Fe surface atoms can have Nd and O neighbours.

Assuming that, first, the hyperfine field enhancement is observed for Fe atoms in the first surface layer (thickness: $e = 0.25$ nm) [18, 19] and, second, that the nanograins are spherical, one can give an estimation of the size of the α-Fe nanograins from the Mössbauer data. The diameter D of a spherical nanograin is related to the volume fraction p_α of bulk α-Fe by:

$$D = \frac{2e}{1 - p_\alpha^{1/3}}.$$

The volume fraction of bulk α-Fe is obtained from the Mössbauer relative absorption areas of the 'α-Fe' and 'mag' components ($\%_\alpha$ and $\%_{mag}$ respectively), assuming that the Lamb–Mössbauer factors of the two contributions (bulk and surface) are equal:

$$p_\alpha = \frac{\%_\alpha}{\%_\alpha + \%_{mag}}.$$

From the Mössbauer spectra of samples oxidized in this work and in [5, 6, 8, 14, 20], the estimated values of D are 6 ± 2 nm in the 150–300 °C range, and 9 ± 2 nm in the 300–400 °C range. At temperatures higher than 450 °C, or at 400 °C for longer times, the mag contribution no longer appears in the Mössbauer spectra of the oxidized powders, indicating that the α-Fe grain size is higher than 100 nm. In figure 6 is shown a high resolution scanning electron micrograph of the oxidized layer of an $Nd_{16}Fe_{76}B_8$ sintered magnet heated at 423 °C for 12 days [20]. Nanograins of 60–100 nm in size can be clearly seen, in agreement with our estimation. These results indicate that the size of the nanograins increases with the oxidation temperature.

The broadening of the α-Fe peak observed in XRD patterns of powders oxidized at temperatures less than 400 °C cannot be explained in terms of grain size effects only, and this confirms the presence of strains, in relation with the presence of interstitial B in the α-Fe grains, which could be responsible for the distorted structure of the α-Fe lattice.

The disappearance of the mag contribution in the Mössbauer spectrum of powders oxidized in the 350–650 °C range can thus be related to the structural change of the α-Fe phase that occurs simultaneously. At 450 °C, the mag contribution disappeared and the α-Fe contribution is fitted with one sextet in agreement with an increase of the α-Fe grain size. The linewidth of the fine sextet is equal to the experimental linewidth (0.26 mm s^{-1}) in agreement with a structural refinement of the grains. This structural refinement can also be evidenced from the evolution of the α-Fe lattice parameter. The lattice parameter deduced from the XRD measurements in powders oxidized at less than 400 °C is higher than that of pure α-Fe in relation with the presence of interstitial B atoms (figure 7). When the oxidation temperature
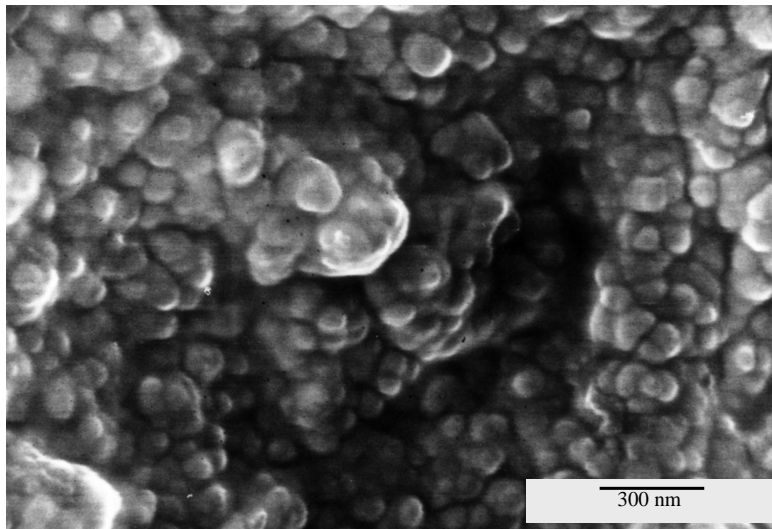
Figure 6. High-resolution scanning electron micrograph of a dissociated grain in an $Nd_{16}Fe_{76}B_8$ sintered magnet heated at 423 °C for 12 days. From [19].
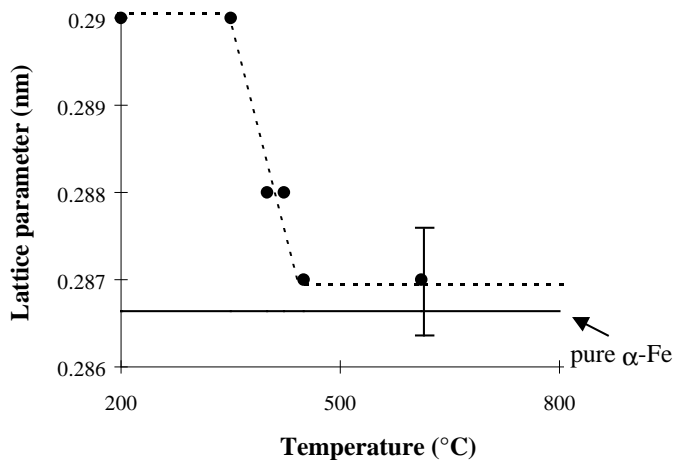

Figure 7. The lattice parameter of the α-Fe phase as a function of the oxidation temperature.

increases, a reduction of the lattice parameter down to the value of pure α-Fe is observed, which corresponds to a sharpening of the α-Fe diffraction peak.

These assumptions are supported by the fact that in the Mössbauer spectrum of an $Nd_{16}Fe_{76}B_8$ powder oxidized at 300 °C for 12 hours and annealed at 600 °C under vacuum for 7 days, the α-Fe contribution is fitted with one fine sextet (figure 8(a)), with a relative absorption area equal to that of the mag and α-Fe contributions together before annealing. It follows that, upon annealing, the growth of the α-Fe grains leads to both a reduction of the relative fraction of the surface atoms and a structural refinement of the grains, that occur simultaneously.
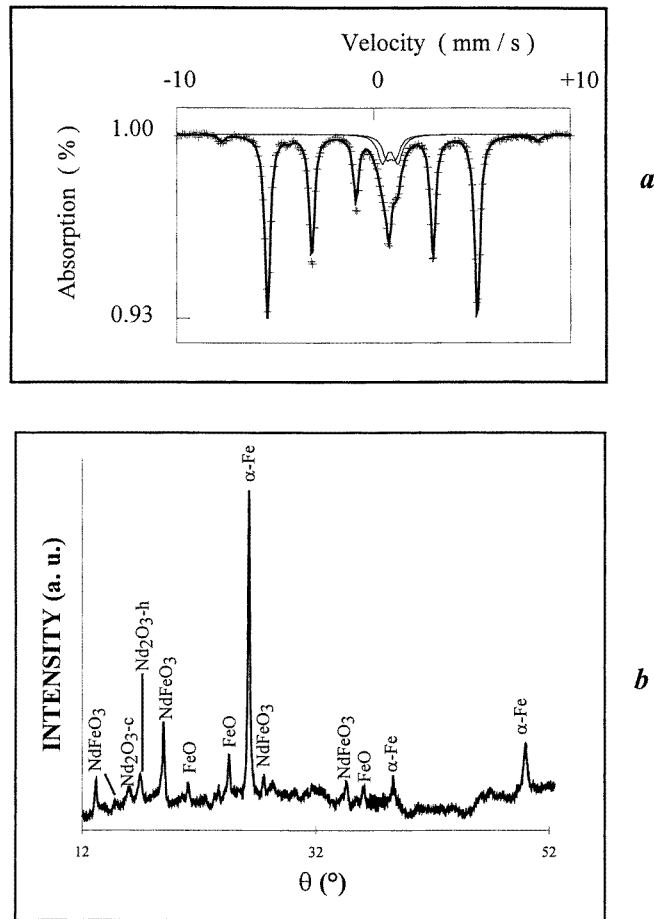
Figure 8. Room temperature Mössbauer spectrum (a) and XRD pattern (b) of the $Nd_{16}Fe_{76}B_8$ powder oxidized at 300 °C for 12 hours and vacuum annealed at 600 °C for 7 days. In the Mössbauer spectrum, the paramagnetic contribution of FeO (two doublets) is displayed.

4.2. The paramagnetic contributions

The room temperature Mössbauer spectrum of the powder oxidized at 300 °C for 12 hours and annealed at 600 °C for 7 days reveals that the para1 contribution disappeared during annealing, the paramagnetic contribution of FeO [21] being present instead (figure 8(a)). The presence of FeO is confirmed by XRD analysis (figure 8(b)). The appearance of FeO is in agreement with the Fe–O phase diagram if one considers that the Fe_3O_4 phase is present in the oxidized powder before annealing: FeO is formed from 570 °C owing to a reaction between α-Fe and Fe_3O_4 according to the following formula [22]:

$$\alpha\text{-Fe} + Fe_3O_4 \rightarrow 4FeO. \tag{1}$$

The FeO compound is stable above 570 °C, and metastable below about 200 °C [22]. The Mössbauer relative areas of the contributions detected in the spectrum of the powder before and after annealing are in complete agreement with reaction (1) if one assumes that the para1 contribution corresponds to Fe_3O_4. The para1 contribution is thus attributed to Fe_3O_4.
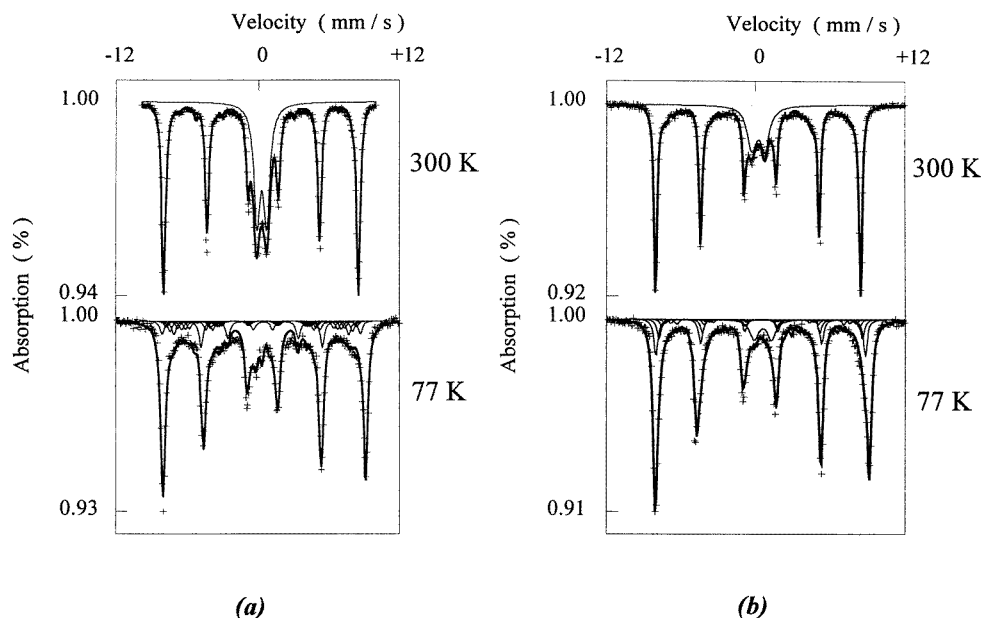
Figure 9. Mössbauer spectra recorded at room temperature and at 77 K of the $Nd_{16}Fe_{76}B_8$ powder oxidized at 400 °C for 7 days (a) and at 600 °C for 2 hours (b). The contribution of para1 is displayed in (a). The contribution of para3 is displayed in (b).

In the 77 K Mössbauer spectrum of the powder oxidized at 400 °C for 7 days (figure 9(a)), no more para1 contribution is observed, and a large magnetic distribution is fitted instead. This behaviour is comparable to that observed in the case of 6 nm Fe_3O_4 nanoparticles at 80 K [23]. The relative area of this magnetic distribution is equal to the relative areas of the para1 and Fe_3O_4 contributions together in the room temperature Mössbauer spectrum. This indicates that the Fe_3O_4 particles related to the para1 contribution are small, being superparamagnetic at room temperature. According to the literature, the behaviour of the Mössbauer spectrum of 6 nm Fe_3O_4 particles is similar to that of para1, and this is not the case for 10 nm Fe_3O_4 particles [23]. The mean size of the Fe_3O_4 particles related to the para1 contribution is thus very probably less than 10 nm.

The 77 K Mössbauer spectrum of the powder oxidized at 600 °C for 2 hours (figure 9(b)) was fitted with the following contributions: α-Fe_2O_3, Fe_3B, a magnetic distribution including the $NdFeO_3$ contribution and para3. The relative area of the para3 contribution is lower at 77 K than at room temperature. This means that the compound corresponding to para3 is paramagnetic at room temperature and partially magnetic at 77 K, thus showing a superparamagnetic behaviour. This compound appears very probably as a distribution of small particles, which could explain the presence of a remaining para3 doublet at 77 K. The room temperature hyperfine parameters of the para3 contribution (see table 2) correspond to those of superparamagnetic α-Fe_2O_3 particles with size less than 10 nm ($\delta = 0.34$ mm s^{-1}, $\Delta = 1.02$ mm s^{-1} estimated from [24], and $\delta = 0.32$ mm s^{-1}, $\Delta = 1.06$ mm s^{-1} after [25]). For this reason, and because the room temperature Mössbauer spectrum of an α-Fe_2O_3 powder with a mean particle size less than 10 nm is paramagnetic [26], the mean size of the superparamagnetic α-Fe_2O_3 particles is estimated here to be less than 10 nm.

From the previous observations, it can be concluded that the transformation of para1 into para3 at 500 °C corresponds to the oxidation of Fe_3O_4 into α-Fe_2O_3 according to the formula:

$$4Fe_3O_4 + O_2 \rightarrow 6\alpha\text{-}Fe_2O_3. \tag{2}$$

The size of these particles does not change significantly upon oxidation, remaining less than 10 nm. The fact that the Fe_3O_4 and α-Fe_2O_3 oxides were not detected by XRD is attributed to the nanometric size of the particles and to the fact that these particles are probably not well crystallized.

The para2 doublet is not clearly identified. Its isomer shift corresponds to the Fe(II) oxidation state, indicating that the related phase contains Fe^{2+} ions. On the other hand, the para2 contribution is still paramagnetic at 77 K, indicating that the related phase is very probably non-magnetic. We therefore assume that the para2 contribution corresponds to Fe^{2+} ions, dispersed in Nd oxides.

5. Discussion

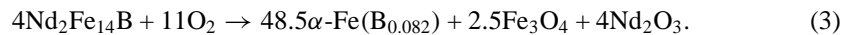### 5.1. The structure of the dissociated $Nd_2Fe_{14}B$ phase

The results of both Mössbauer and XRD investigations are consistent and show that at temperatures lower than 400 °C, the structure of the dissociated $Nd_2Fe_{14}B$ phase consists in α-Fe nanograins (less than 10 nm in size, with a distorted structure) and Fe_3O_4 superparamagnetic particles (less than 10 nm in size), mixed with amorphous or poor crystallized Nd_2O_3 regions. This structure is outlined in figure 10. The presence of superparamagnetic Fe_3O_4 is related to the oxidation of the Nd in the $Nd_2Fe_{14}B$ phase: the reaction between the Nd atoms and oxygen releases enough energy to oxidize the Fe atoms in their close vicinity, forming very small Fe_3O_4 particles that are embedded in Nd_2O_3 regions (thus showing a superparamagnetic behaviour). This interpretation is consistent with TEM observations of an Nd–Dy–Fe–Co–V–Al–B magnet oxidized at 110 °C for 120 hours [9] and indicates that the size of the α-Fe nanograins depends on the temperature, being 2 nm at 110 °C [9], 6 nm in the 150–300 °C range and 9 nm in the 300–400 °C range. The α-Fe nanograins are organized in domains (about 100 nm in size) with the same crystallographic orientation, as shown by TEM observations [9].

From 400 °C, a change in the structure of the α-Fe phase is observed: a structural refinement and a growth of the α-Fe grains occur simultaneously. Thus at 400 °C for long times (several days) or at temperatures higher than 450 °C, the microstructure of the dissociated phase is constituted of bigger α-Fe grains (their size being 100 nm or more), Fe_3O_4 precipitates (size less than 10 nm) and crystallized h-Nd_2O_3 precipitates. The growth of the α-Fe grains probably results from the coalescence of the α-Fe nanograins having the same crystallographic orientation. This structure is outlined in figure 10. This interpretation is consistent with TEM observations of an Nd–Fe–B magnet oxidized at 423 °C for 12 days [10].

Consequently, the TEM observations mentioned in section 1 [9, 10] are not inconsistent, but reflect the influence of the oxidation temperature on the structure of the dissociated $Nd_2Fe_{14}B$ phase.

5.2. The oxidation reactions

According to the relative absorption areas of α-Fe and Fe_3O_4 deduced from the Mössbauer spectra, the following reaction can be written:

$$4Nd_2Fe_{14}B + 11O_2 \rightarrow 48.5\alpha\text{-}Fe(B_{0.082}) + 2.5Fe_3O_4 + 4Nd_2O_3. \tag{3}$$
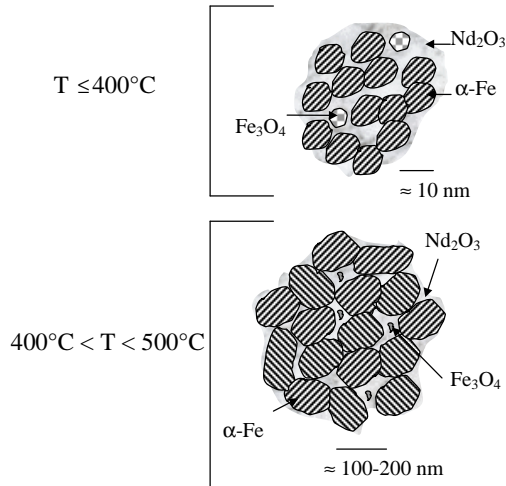
Dissociated layer

Figure 10. Schematic microstructure of the dissociated $Nd_2Fe_{14}B$ phase as a function of the oxidation temperature. The common orientation of the α-Fe nanograins for $T \leqslant 400\,°C$ is evidenced.

Considering the global atomic composition of a dissociated grain ($Nd_{8.8}Fe_{62.2}B_{4.5}O_{24.5}$), the amount of oxygen obtained from this reaction is very consistent with electron probe microanalysis measurements of the composition of the dissociated grains in bulk samples oxidized at $423\,°C$ ($Nd_{9\pm1}Fe_{60\pm3}B_{4\pm1}O_{27\pm3}$) [6].

During further oxidation, several reactions occur that depend on the oxidation temperature. For temperatures less than $500\,°C$, the α-Fe grains are oxidized first into Fe_3O_4 and then into α-Fe_2O_3 according to:

$$3\alpha\text{-Fe} + 2O_2 \rightarrow Fe_3O_4 \tag{4}$$

and to reaction (2), and their magnetic contributions are detected in the Mössbauer spectra. The oxidation proceeds from the surface of the particle to its inner part, as shown in figure 11, due to the diffusion of oxygen within the oxide layer. The fact that the contribution of superparamagnetic Fe_3O_4 is still observed is attributed to a faster diffusion of oxygen through the α-Fe_2O_3 grains than through the Nd_2O_3 amorphous regions (the Nd_2O_3 amorphous regions act for the Fe_3O_4 nanoparticles as a protective layer against oxidation).

For temperatures higher than $500\,°C$, the same reactions occur due to the diffusion of oxygen into the particle, as shown in figure 12. The superparamagnetic α-Fe_2O_3 contribution is observed instead of Fe_3O_4 due to the oxidation of the nanoparticles of Fe_3O_4 formed in the Nd_2O_3 regions into α-Fe_2O_3 according to formula (2). This is attributed to the diffusion of oxygen through the h-Nd_2O_3 regions at these temperatures, in relation with the structural change of the Nd_2O_3 amorphous regions at $500\,°C$ (see section 3.2). The $NdFeO_3$ contribution is detected in the Mössbauer spectra. As this phase forms owing to the following reaction between Nd_2O_3 and α-Fe_2O_3:
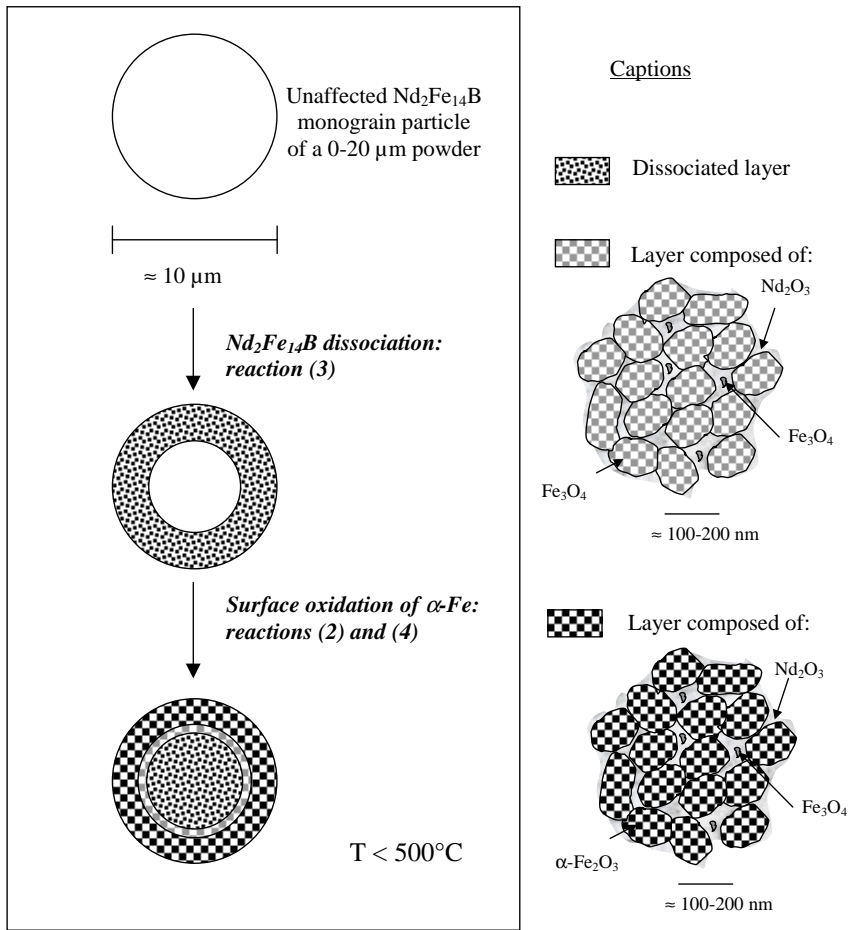
$$\alpha\text{-}Fe_2O_3 + Nd_2O_3 \rightarrow 2NdFeO_3 \tag{5}$$

Figure 11. The oxidation process of an $Nd_2Fe_{14}B$ particle at temperatures less than 500 °C.

it is concluded that $NdFeO_3$ regions form at the Nd_2O_3/α-Fe_2O_3 interfaces. The α-Fe_2O_3 precipitates in the Nd_2O_3 regions probably transform in $NdFeO_3$ as well.

The reactions (2), (4) and (5) are in agreement with the Mössbauer relative areas of the different phases deduced from the Mössbauer spectra of the oxidized powders. All these results, obtained for Nd–Fe–B powders, are consistent with the investigation of the oxidation of bulk Nd–Fe–B magnets at high temperature [6].

The dissociation of the $Nd_2Fe_{14}B$ phase being well characterized for the $Nd_{16}Fe_{76}B_8$ powdered magnet, the influence of additives on the dissociation process was investigated for Nd–Fe–B powders containing additives.

6. Oxidized Nd–Fe–B powders containing additives

The nominal atomic compositions of the samples containing additives (DCVA, CVA, CMA and DNA) are reported in table 1. The microstructural investigation of these samples is reported elsewhere [27]. This study revealed the presence of both intergranular and intragranular
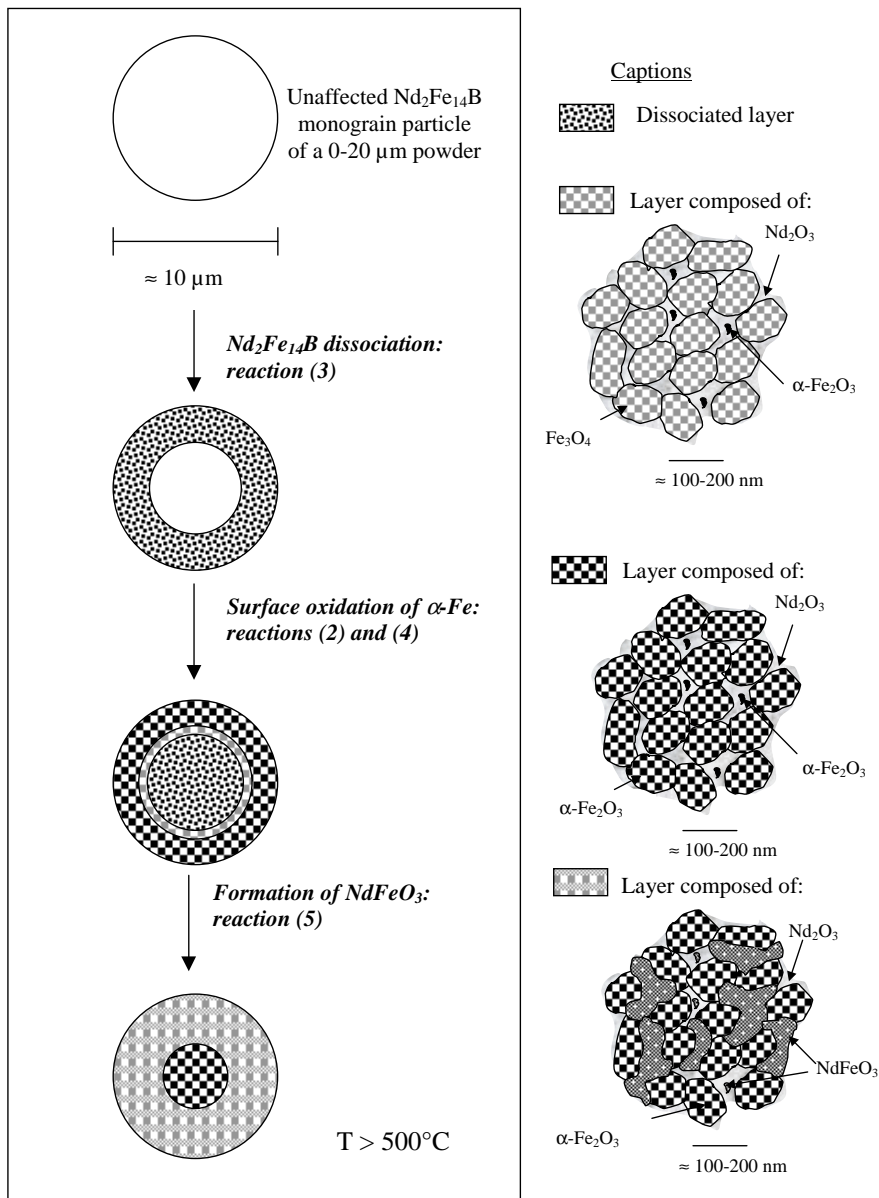
Figure 12. The oxidation process of an Nd$_2$Fe$_{14}$B particle at temperatures higher than 500 °C.

X–Fe–B precipitates (with X = V, Nb, Mo). These phases were found to be corrosion resistant in the 200–300 °C temperature range. The Mössbauer spectra of the fully oxidized DCVA, CVA and CMA samples are very similar, and were fitted with the same contributions (in the same proportions, within the experimental accuracy). The spectrum of the CMA sample is shown in figure 13, and the hyperfine parameters of the contributions used to fit the spectrum are reported in table 3. On the other hand, the Mössbauer spectrum of the fully oxidized DNA sample is very similar to that of the fully oxidized Nd$_{16}$Fe$_{76}$B$_8$ sample.
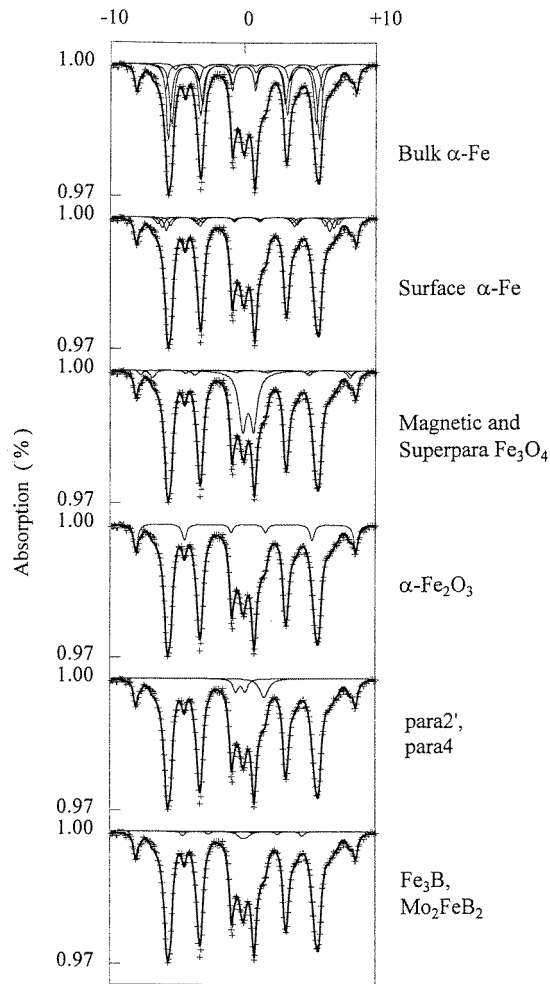
Figure 13. Room temperature Mössbauer spectrum of the CMA powder oxidized at 300 °C for 3 days. The contributions used to fit the spectrum are displayed.

The $Nd_2Fe_{14}B$ phase is fully dissociated as its contribution no longer appears. For each sample, a paramagnetic contribution attributed to the corrosion-resistant X–Fe–B phase is fitted. Concerning the dissociation products, the same contributions as in the spectra of oxidized samples with no additives are fitted (bulk and surface contributions of α-Fe, α-Fe_2O_3, magnetic and superparamagnetic Fe_3O_4 and a paramagnetic contribution attributed to Fe^{2+} ions in Nd oxides). Other contributions (Fe_3B and para4) are fitted in the Co containing samples.

As for the $Nd_{16}Fe_{76}B_8$ powder oxidized at 300 °C for 12 hours, the main contribution (fitted with a discrete distribution of hyperfine fields) corresponds to α-Fe. However, for the DCVA, CVA and CMA samples, the α-Fe contribution is characterized by a higher mean hyperfine field (34.6–34.7 T) than that obtained for the $Nd_{16}Fe_{76}B_8$ and DNA samples (33.3–33.4 T). This is attributed to the presence of Co in the α-Fe phase, in agreement with the fact that Co atoms substitute for Fe atoms in the $Nd_2Fe_{14}B$ unit cell [27]. By interpolating the results

Table 3. Hyperfine parameters and Mössbauer relative intensities ($\pm1\%$) of the contributions to the Mössbauer spectrum of the CMA powder oxidized at 300 °C for 3 days. * means that the contribution was fitted using a distribution of hyperfine fields (B is the mean hyperfine field). The hyperfine parameters for Fe$_3$O$_4$ were fixed to the values obtained from the literature [15]. The hyperfine parameters for Fe$_3$B were fixed to the values obtained for the Nd$_{16}$Fe$_{76}$B$_8$ oxidized sample.

Contribution	δ (mm s^{-1})	2ε, Δ (mm s^{-1})	B (T)	Relative absorption area (%)
bulk α-Fe (distribution)	0.05 ± 0.02	0.01 ± 0.02	34.7	56*
surface α-Fe (distribution)	0.34 ± 0.02	-0.08 ± 0.02	38.7	13*
α-Fe$_2$O$_3$	0.35 ± 0.04	-0.16 ± 0.05	51.2 ± 0.2	7
Fe$_3$O$_4$	0.26	-0.16	49.0	4
	0.67	-0.20	46.0	
Fe$_3$B	0.01	0.00	27.8	2
	-0.09	0.00	26.2	
	0.11	0.00	22.6	
superpara Fe$_3$O$_4$	0.41 ± 0.03	0.84 ± 0.04	—	11
para2$'$	1.65 ± 0.03	0.02 ± 0.04	—	3
para4	-0.15 ± 0.03	0.70 ± 0.04	—	2
Mo$_2$FeB$_2$	0.09 ± 0.01	0.37 ± 0.01	—	2

of a study of the mean hyperfine field in Fe$_{1-x}$Co$_x$ compounds (with $0 \leqslant x \leqslant 0.5$) [28], the Co content in α-Fe was estimated to be 8 at.%. A similar effect is observed for the mag contribution, in agreement with the fact that this contribution corresponds to the surface atoms in the α-Fe grains.

The fact that the Fe$_3$B and para4 contributions are not observed in the spectrum of oxidized Nd$_{16}$Fe$_{76}$B$_8$ or DNA powders is attributed to the presence of Co in the Nd$_2$Fe$_{14}$B phase, which leads to the formation of other dissociation products (in weak proportions) during the dissociation process. The formation of some Fe$_3$B during the process could be related to the fact that the Co content in the α-Fe phase (8 at.%) is higher than in the Nd$_2$Fe$_{14}$B phase (5 at.% [27]). The para4 contribution, in very weak amount, remains unidentified.

It appears that the presence of additives in sintered Nd–Fe–B magnets does not change the dissociation process. Apart from some contributions in very weak proportions in Co containing samples, the same contributions appear, owing to the same reactions. This is consistent with the fact that the activation energy of the dissociation reaction is the same for samples with and without additives [27].

7. Summary and conclusion

The dissociation process of the Nd$_2$Fe$_{14}$B phase in a sintered Nd$_{16}$Fe$_{76}$B$_8$ powdered magnet was studied between 300 and 650 °C. The oxidized powders were analysed by Mössbauer spectrometry and x-ray diffraction. In the 300–350 °C temperature range, the main dissociation product is α-Fe, which results from the oxidation of Nd in the Nd$_2$Fe$_{14}$B phase. It was shown that the α-Fe phase appears as nanograins. In the 350–650 °C temperature range, the Nd$_2$Fe$_{14}$B dissociation process going very fast, the oxidation of the α-Fe phase is mainly observed. The

characterization of the oxidation reactions occurring at high temperature allowed us to identify the dissociation products accurately. The results were interpreted consistently with previous TEM observations and the microstructure of the dissociated phase was thus characterized accurately as a function of the oxidation temperature.

For temperatures less than $400\,°C$, the microstructure consists in α-Fe nanograins (less than 10 nm in size, with a distorted structure) and Fe_3O_4 superparamagnetic particles (about 6 nm in size), mixed with amorphous or poorly crystallized Nd_2O_3 regions. For temperatures higher than $400\,°C$ (or at $400\,°C$ for several days) the microstructure consists in bigger α-Fe grains (their size being 100 nm or more), Fe_3O_4 precipitates (size less than 10 nm) and crystallized h-Nd_2O_3 precipitates.

From the Mössbauer measurements, a dissociation reaction was proposed for the $Nd_2Fe_{14}B$ phase which is consistent with previous EPMA measurements. The oxidation reactions occurring at high temperatures are in agreement with the relative intensities deduced from the Mössbauer analyses as well.

The dissociation process was investigated for Nd–Fe–B powders containing additives. It was found that the presence of additives in sintered Nd–Fe–B magnets does not change significantly the dissociation process.

Acknowledgments

References

[1]   Tenaud P, Vial F and Sagawa M 1990 *IEEE Trans. Magn.* **26** 1930
[2]   Tokuhara K and Hirosawa S 1991 *J. Appl. Phys.* **69** 5521
[3]   Camp F E and Kim A S 1991 *J. Appl. Phys.* **70** 6348
[4]   Blank R and Adler E 1987 *Proc. 9th Int. Workshop on Rare Earth Magnets and their Applications (31 August–2 September 1987, Bad Soden, Germany)* ed C Herget and P Poerschke (Bad Honnef: DPG e.V.) p 537
[5]   Le Breton J M, Teillet J, McGuinness P, Edgley D S and Harris I R 1992 *IEEE Trans. Magn.* **28** 2157
[6]   Edgley D S, Le Breton J M, Steyaert S, Ahmed F M, Harris I R and Teillet J 1997 *J. Magn. Magn. Mater.* **173** 29
[7]   Cygan D F and McNallan M J 1995 *J. Magn. Magn. Mater.* **139** 131
[8]   Le Breton J M and Teillet J 1990 *IEEE Trans. Magn.* **26** 2652
[9]   Legras L 1994 *PhD Thesis* Université de Rouen
[10] Edgley D S, Le Breton J M, Lemarchand D, Harris I R and Teillet J 1993 *J. Magn. Magn. Mater.* **128** L1
[11] Teillet J and Varret F 1983 unpublished MOSFIT program
[12] Grandjean F, Long G J, Tharp D E, Pringle O A and James W J 1988 *J. Physique Coll.* **49** C8 581
[13] Niarchos D, Zouganelis G, Kostikas A and Simopoulos A 1986 *Solid State Commun.* **59** 389
[14] Steyaert S, Le Breton J M and Teillet J 1996 *J. Phys.: Condens. Matter* **8** 10 721
[15] Murad E and Johnston J H 1987 *Mössbauer Spectroscopy Applied to Inorganic Chemistry* vol 2, ed G J Long (New York: Plenum) p 507
[16] Bagayoko D and Callaway J 1983 *Phys. Rev.* B **28** 5419
[17] Ohnishi S, Weinert M and Freeman A J 1984 *Phys. Rev.* B **30** 36
[18] Liu G and Gradmann U 1993 *J. Magn. Magn. Mater.* **118** 99
[19] Dormann J L, Fiorani D and Tronc E 1997 *Adv. Chem. Phys.* **98** 283
[20] Le Breton J M 1992 *PhD Thesis* Université de Rouen
[21] Johnson D P 1969 *Solid State Commun.* **7** 1785
[22] Schecter H, Hillman P and Ron M 1966 *J. Appl. Phys.* **37** 3043
[23] Morup S, Topsoe H and Lipka J 1976 *J. Physique Coll.* **37** C6 287
[24] Nakamura T, Shinjo T, Endoh Y, Yamamoto N, Shiga M and Nakamura Y 1964 *Phys. Lett.* **12** 178

[25] Constabaris G, Lindquist R and Kündig W 1965 *Appl. Phys. Lett.* **7** 59
[26] Kündig W, Bömmel H, Constabaris G and Lindquist R 1966 *Phys. Rev.* **142** 327
[27] Steyaert S, Le Breton J M and Teillet J 1998 *J. Phys. D: Appl. Phys.* **31** 1534
[28] Fultz B, Hamdeh H and Okamoto J 1990 *Hyperfine Interact.* **54** 799